Dual Mach-Zehnder Interferometer Based on DCF and FCF for Temperature and Strain Measurement

Ya GAO[1,2], Shu JIN[1,2], Cheng ZUO[1,2], Benli YU[1,2], and Shenglai ZHEN[1,2*]

[1]*Key Laboratory of Opto-Electronic Information Acquisition and Manipulation of Ministry of Education, Anhui University, Hefei 230601, China*

[2]*Information Materials and Intelligent Sensing Laboratory of Anhui Province, Anhui University, Hefei 230601, China*

[*]Corresponding author: Shenglai ZHEN E-mail: slzhen@ahu.edu.cn

Abstract: In this paper, a dual Mach-Zehnder interferometer for measuring both temperature and strain is proposed and verified by experiments. The sensor configuration involves cascading a four-core fiber and a double-clad fiber between two single-mode fibers. By exploiting the different responses of the two Mach-Zehnder interferometers to temperature and strain, we construct a matrix using two selected resonance dips from the transmission spectra, so that both temperature and strain can be measured simultaneously. The experimental results show the sensor's remarkable performance, with the maximum temperature sensitivity of −94.2 pm/℃ and the maximum strain sensitivity of 2.68 pm/με. The maximum temperature error and strain error are found to be ±0.35 ℃ and ±4.8 με, respectively. Compared with other optical fiber sensors, the sensor has high sensitivity, a simple structure, and ease to manufacture and implement, making it a structure choice for applications in quality inspection of materials.

Keywords: Dual Mach-Zehnder interferometer; temperature; strain

Citation: Ya GAO, Shu JIN, Cheng ZUO, Benli YU, and Shenglai ZHEN, "Dual Mach-Zehnder Interferometer Based on DCF and FCF for Temperature and Strain Measurement," *Photonic Sensors*, 2025, 15(1), 250120.

1. Introduction

Compared with the traditional electrical sensors, optical fiber sensors (OFSs) find wide-ranging applications in various fields, including the temperature [1, 2], magnetic field [3], pressure [4], and refractive index [5], due to their advantages of the compact size, high sensitivity, and strong resistance to electromagnetic interference. In recent years, several types of OFSs such as Fabry-Perot interferometers (FPIs) [6], fiber Bragg grating (FBG) sensors [7], and fiber-optic gyroscopes (FOGs) [8] have gradually found practical applications.

In scenarios such as engines, civil engineering, and chemical plants, where heating or cooling frequently occurs, measuring strain and temperature in structural materials simultaneously becomes critical. OFSs [9, 10] are capable of simultaneous temperature and strain measurement, and play an important role in these scenarios. Previously, researchers often utilized FBG for this dual sensing purpose. However, its sensitivity is limited to approximately 10 pm/℃ [11]. The use of the advanced processing technology [12] or coated sensitive materials [13, 14] is expected to further improve the sensitivity of OFSs.

In recent years, multi-core optical fibers (MCFs) have garnered significant attention and started to be

Received: 9 October 2023 / Revised: 16 February 2024

DOI: 10.1007/s13320-024-0735-z
Article type: Regular

applied in the sensing field due to their high communication capacity and high integration [15]. A Mach-Zehnder interferometer (MZI) based on a tapered four-core fiber (TFCF) cascade FBG was proposed by W. Feng *et al*. [16]. The cascade sensors are complex, and FBGs are expensive and inherently cross-sensitive. Subsequently, J. Tian *et al*. [17] proposed hollow-core tube fibers (HTFs) based on the cascaded FPI for temperature and strain dual covariate measurement but encountered significant FPI losses. S. Xiao *et al*. [18] presented a fiber-optic MZI sensor in 2022, which contained three peanut cones, a standard single-mode fiber (SMF), and a commercially available panda-type polarization-maintaining fiber (PMF). In the following year, an improved structure cascaded two portions of the standard SMF through the three peanut cones [19], achieving the temperature sensitivity of 78.29 pm/℃ and the strain sensitivity of −0.639 pm/με. To achieve the higher sensing sensitivity, J. Ruan *et al.* [20] attempted to sandwich a section of the PMF between a multimode fiber (MMF) and a double-hole fiber (DHF) to fabricate a sensor based on the MZI and the Sagnac loop in 2023. His structure significantly improved the temperature and strain sensitivity of the sensor, but the overall fiber length was large, prompting the need for a miniaturized temperature-strain dual parametric sensor. In the same year, researchers fused two types of fibers, a thin-core fiber (TCF) and a small cladding polarization-maintaining fiber (SCPMF), with core offsets to create a dual MZI capable of simultaneous temperature and strain measurement. The sensor is characterized by its low cost, responsiveness, and miniaturized design, but the fusion spliced with a core offset is susceptible to breakage [21].

The above sensors have simple structures and have been applied, but in the field of civil engineering quality inspection, higher requirements are put forward for the high sensitivity and low error of optical fiber sensors. In this paper, a double MZI sensor based on a cascade of the four-core fiber (FCF) and double-clad fiber (DCF) is proposed for the simultaneous measurement of temperature and strain. The sensor operates by tapering an FCF between two SMFs as the first MZI, followed by cascading a segment of the DCF behind the FCF to create the second MZI. The sensor is stable in structure and easy to manufacture. Through experimental demonstrations, it is shown that the two transmission spectrum dips can be utilized to establish a dual covariance matrix for the simultaneous measurement of temperature and strain. The sensors offer a new alternative to temperature strain sensors by eliminating the need for expensive and complex processing and by being structurally stable and highly sensitive.

2. Principle of the sensor

The sensor structure is depicted in Fig. 1. As the optical signal enters the FCF from the input SMF through the taper, a portion of the light is coupled into the four cores of the FCF, while the other part of the light is excited into the cladding, forming a cladding mode. Upon reaching the DCF, the light inside the fiber cores and the light inside the cladding interfere with the difference in the optical path length, resulting in the formation of the first MZI at the fusion point of the FCF and the DCF.

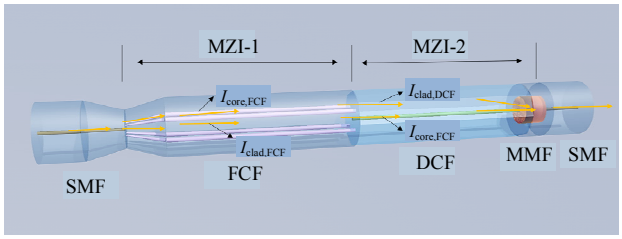

Fig. 1 Schematic diagram of the sensor.

The light intensity at the first MZI can be expressed as [22]

$$I_1 = I_{\text{core,FCF}} + I_{\text{clad,FCF}} + 2\sqrt{I_{\text{core,FCF}} I_{\text{clad,FCF}}}\cos\left(\frac{2\pi\Delta n_{\text{eff},1} L_1}{\lambda}\right). \quad (1)$$

Subsequently, a portion of the light energy in the FCF enters the cladding of the DCF and gets excited

once more, while the other portion of the light energy enters the fiber core of the DCF. The two modes of light continue to propagate forward into the MMF, which acts as a coupler in the sensor. The two beams are coupled into the SMF, then interfere again to form the second MZI.

The light intensity at the second MZI can be expressed as

$$I_2 = I_{\text{core,DCF}} + I_{\text{clad,DCF}} + 2\sqrt{I_{\text{core,DCF}} I_{\text{clad,DCF}}}\cos\left(\frac{2\pi\Delta n_{\text{eff},2} L_2}{\lambda}\right) \tag{2}$$

$$I_{\text{core,FCF}} = \gamma_1\alpha_1 I_0 \tag{3}$$

$$I_{\text{clad,FCF}} = (1-\gamma_1) I_0 \tag{4}$$

$$I_{\text{core,DCF}} = \gamma_2\alpha_2 I_1 \tag{5}$$

$$I_{\text{clad,DCF}} = (1-\gamma_2) I_1 \tag{6}$$

where $I_{\text{core,FCF}}$ represents the light intensity inside the FCF core, $I_{\text{clad,FCF}}$ is the light intensity inside the FCF cladding, $I_{\text{core,DCF}}$ denotes the light intensity inside the DCF core, $I_{\text{clad,DCF}}$ is the light intensity inside the DCF cladding. $\Delta n_{\text{eff},1}$ is the effective refractive index difference between the core and cladding in the FCF, $\Delta n_{\text{eff},2}$ is the effective refractive index difference between the core and cladding in DCF, L_1 and L_2 are the lengths of the FCF and DCF, respectively, I_0 signifies the emitted light intensity, γ_1 and γ_2 are the ratios of the light intensity in the split to the total light intensity in the fiber core, and α_1 and α_2 are the propagation loss results.

When the phase difference satisfies $\varphi=(2j+1)\pi$ and $\varphi'=(2j'+1)\pi$, the wavelength of the interference peaks and valleys can be expressed as

$$\lambda_j = \frac{2\Delta n_{\text{eff},1} L_1}{(2j+1)} \tag{7}$$

$$\lambda_{j'} = \frac{2\Delta n_{\text{eff},2} L_2}{(2j'+1)} \tag{8}$$

where j and j' represent integers, φ and φ' represent the phase difference between the two interferometers, respectively. When the external temperature and strain undergo changes, the wavelength corresponding to the dips will also be affected accordingly. In order to measure the strain and temperature, at least two dips are chosen to measure their wavelength displacements. The wavelengths of the dips with changes in the temperature and strain can be expressed as follows:

$$\begin{aligned}\Delta\lambda_j &= \lambda_j\left[(\xi_1+\alpha_1)\Delta T + (1-P_{\xi,1})\Delta\varepsilon\right] \\ &= K_{jT}\Delta T + K_{j\varepsilon}\Delta\varepsilon\end{aligned} \tag{9}$$

$$\begin{aligned}\Delta\lambda_{j'} &= \lambda_{j'}\left[(\xi_2+\alpha_2)\Delta T + (1-P_{\xi,2})\Delta\varepsilon\right] \\ &= K_{j'T}\Delta T + K_{j'\varepsilon}\Delta\varepsilon\end{aligned} \tag{10}$$

where ξ_1 and ξ_2 are the thermo-optic coefficients, α_1 and α_2 are the coefficients of thermal expansion, $P_{\xi,1}$ and $P_{\xi,2}$ are the effective elastic-optic coefficients, K_{jT} and $K_{j\varepsilon}$ are the temperature sensitivity and strain sensitivity of the first MZI, $K_{j'T}$ and $K_{j'\varepsilon}$ are the temperature sensitivity and strain sensitivity of the second MZI.

From the above equation, the temperature sensitivity and strain sensitivity matrix can be expressed as

$$\begin{pmatrix}\Delta T \\ \Delta\varepsilon\end{pmatrix} = \begin{pmatrix}K_{1T} & K_{1\varepsilon} \\ K_{2T} & K_{2\varepsilon}\end{pmatrix}^{-1}\begin{pmatrix}\Delta\lambda_1 \\ \Delta\lambda_2\end{pmatrix} = \frac{1}{(K_{2\varepsilon}K_{1T} - K_{2T}K_{1\varepsilon})}\begin{pmatrix}K_{2\varepsilon} & -K_{1\varepsilon} \\ -K_{2T} & K_{1T}\end{pmatrix}\begin{pmatrix}\Delta\lambda_1 \\ \Delta\lambda_2\end{pmatrix}. \tag{11}$$

3. Fabrication of the sensor

The FCF (FIBERCORE, SM-4C1500) used is shown in Fig. 2(a), with the four cores of the fiber arranged in a matrix with a core spacing of 50 μm, a core diameter of 8 μm, and a cladding diameter of 125 μm. The DCF (CORACTIVE, DCF-EY-10/128H) used is shown in Fig. 2(c), with a core diameter of 10 μm and a cladding diameter of 128 μm. The microscopic images of the fusion points between the SMF and FCF are displayed in Fig. 2(b), and the microscopic images of the fusion points between the FCF and DCF are shown in Fig. 2(d).

The manufacturing process of the sensor is shown in Fig. 3. Firstly, a fusion splicer (Fujikura FSM-100P+) is used to fuse the SMF at one end of the FCF. The splicer has the ability to taper the fiber

with the special function. The optimum fusion parameters are determined by repeated experiments: the main fusion power is 60 bits; the discharge time is 1400 ms; the fiber feeding speed is 0.50 μm/ms. The wrist diameter at the fusion point is 85 μm and the length of the taper section is 1 mm. Subsequently, the fiber is cut by using a fiber cleaver and the FCF end is flat cut. Next, a section of the DCF is fused at the other end of the FCF by using automatic discharge. Following this, an MMF with a length of 1 mm is fused with the DCF. Finally, the SMF is fused at the other end of the MMF, and the sensor is completed.

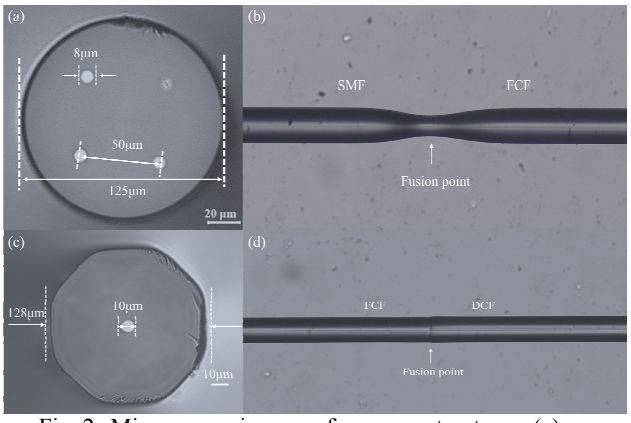

Fig. 2 Microscope image of sensor structure: (a) cross section of the FCF, (b) fusion point of the SMF and FCF, (c) cross section of the DCF, and (d) fusion point of the FCF and DCF.

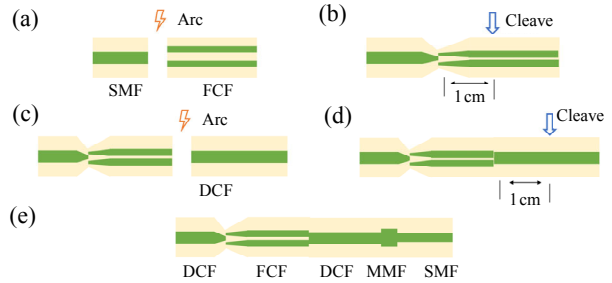

Fig. 3 Fabrication process of the sensor: (a) fusing the SMF with the FCF, (b) flat cutting the FCF end, (c) fusing the FCF with the DCF, (d) flat cutting the FCF end, and (e) fusing the DCF with the MMF.

The spatial spectral diagram is obtained by using the fast Fourier transform (FFT) method, as shown in Fig. 4. We make three sensors with different fiber lengths. The main spatial frequency of Fig. 4(a) is 0.074 99 nm^{-1}, and the main spatial frequency of Fig. 4(b) is 0.03999 nm^{-1}, which is mainly caused by the different lengths of the DCF. The dominant spatial frequencies in Figs. 4(a) and 4(c) are both 0.074 99 nm^{-1} and the remaining spatial frequency corresponds to other weak interference modes. The relationship among the spatial frequency ξ, the interference length L, and the effective emissivity difference Δn is expressed as

$$\xi = \frac{\Delta nL}{\lambda^2}. \tag{12}$$

The effective refractive index difference of the DCF is 0.012, which corresponds to its numerical aperture of 0.2, and it can be demonstrated that the interference between the core and cladding modes of the MZI-2 introduces the dominant spatial frequency.

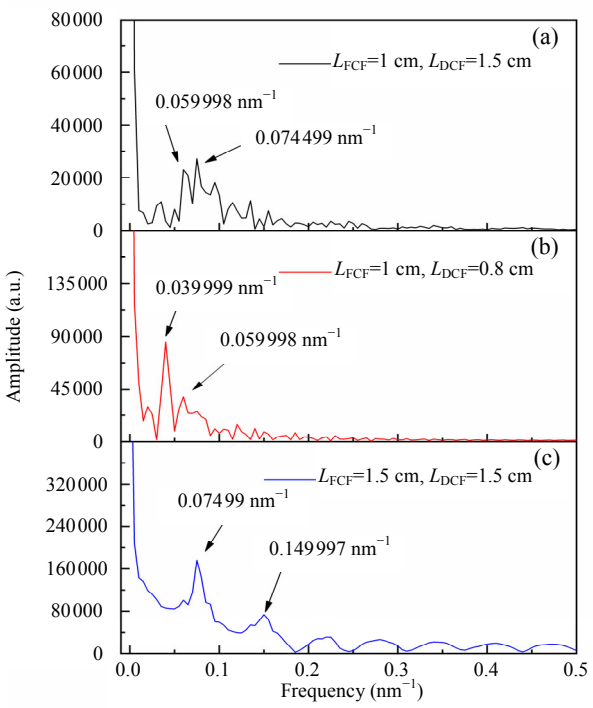

Fig. 4 Spatial frequency spectra of sensors fabricated with different lengths of the fiber: (a) L_{FCF}=1 cm, L_{DCF}=1.5 cm, (b) L_{FCF}=1 cm and L_{DCF}=0.8 cm, and (c) L_{FCF}=1.5 cm and L_{DCF}=1.5 cm (where L_{FCF} is the length of the FCF, and L_{DCF} is the length of the DCF).

4. Experiments and analysis

4.1 Temperature response

The temperature experimental setup is shown in Fig. 5. Light emitted through an ultra-wideband light

source (UWBLS, Go-light, 1250 nm–1650 nm) enters the sensor. The sensing unit is fixed on the high precision temperature measurement (Sunny Precise, SLD70), the resolution of 0.001 ℃, and the optical spectrum analyzer (OSA, YOKOGAWA, AQ6370D) records the output spectra.

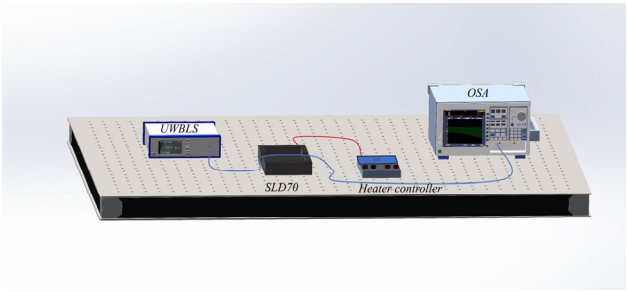

Fig. 5 Schematic of the temperature measurement setup.

In the temperature experiment, the experimental setup is kept stable, and the temperature change gradient is controlled at 5 ℃. The transmission spectra are measured in the range of 25 ℃–55 ℃, and each temperature being maintained for twenty minutes. The measured transmission spectra under different temperatures and the dip wavelengths versus temperature are shown in Fig. 6(a). The insertion loss is approximately 12 dB, and the spectra show a blueshift as the temperature increases. The blueshift of the resonant wavelength is attributed to the negative thermo-optical coefficient of the fiber. Figure 6(b) presents the temperature response of the two selected dips and their corresponding blueshifts: the blueshifts of the two dips are 2.85 nm and 2.32 nm, respectively. The temperature sensitivity is found to be −94.2 pm/℃ and −78.38 pm/℃, respectively. Data fitting shows the linear relationship between the temperature and wavelength. The values of the fitting linearity are 99.715% and 99.808%, respectively.

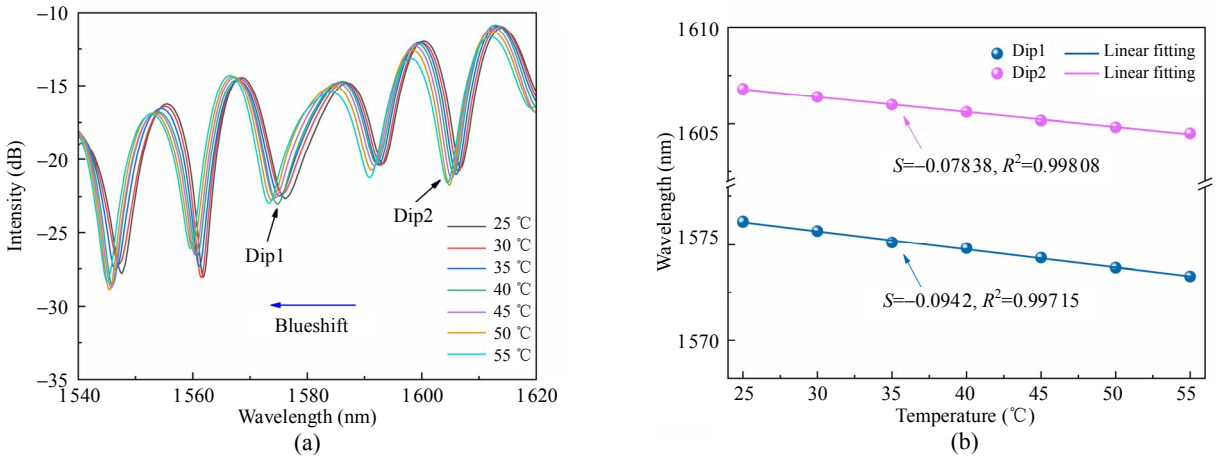

Fig. 6 Temperature sensing experimental results: (a) measured transmission spectra under different temperatures and (b) dip wavelengths versus temperature.

4.2 Strain response

The strain experimental setup is depicted in Fig. 7. The light source and OSA used are the same as those employed in the temperature measurement. The sensor is naturally straightened, with one end fixed on the electric displacement table using the ultraviolet (UV) glue, while the other end is fixed on the double-hole plate. As the stepping motor moves, an axial strain is applied to the sensor. The minimum travel distance of the motorized displacement stage is 0.01 mm, and the initial distance between the two platforms is 20 cm. The computer can control the movement of the unidirectional stepper motor. The strain applied to the sensor is calculated as $\varepsilon=\Delta L/L$ (where ΔL represents the length of the fiber being stretched, that is, the distance that the stepper motor is moving, and L is the total fiber length between the two segments).

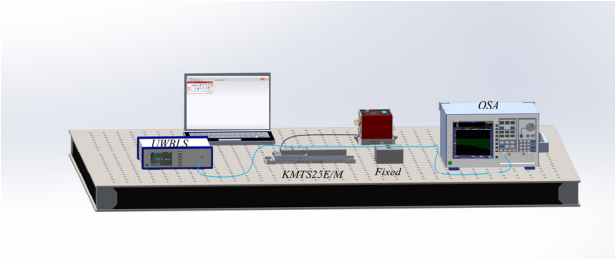

Fig. 7 Schematic of the strain measurement setup.

Strain sensing experiments are carried out at room temperature, controlling the gradient of strain change to 500 με. Figure 8(a) illustrates the spectra response with strain ranging from 0 με to 3000 με at intervals of 500 με. As the strain increases, the spectra experience a redshift, and the sensor fractures when the strain reaches 3500 με. Figure 8(b) shows the strain response of the two selected dips, along with the redshift of two dips measuring 6.69 nm and 3.86 nm, respectively. The strain sensitivity is calculated as 2.68 pm/με and 1.53 pm/με, respectively. The values of the fitting linearity are 99.474% and 99.974%, respectively.

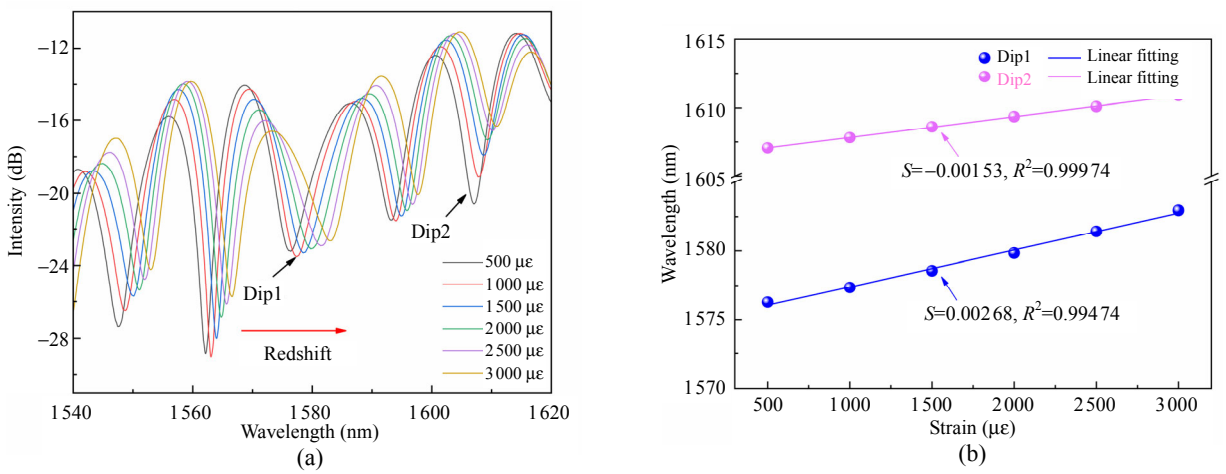

Fig. 8 Strain sensing experimental results: (a) measured transmission spectra under different strains and (b) dip wavelengths versus strain.

The temperature strain sensitivity matrix is constructed using the two dips, which is denoted as

$$\begin{pmatrix}\Delta T\\ \Delta\varepsilon\end{pmatrix}=\frac{1}{65.932\ 4}\begin{pmatrix}1.53 & -2.68\\ 78.38 & -94.2\end{pmatrix}\begin{pmatrix}\Delta\lambda_1\\ \Delta\lambda_2\end{pmatrix}. \quad (13)$$

Since the minimum resolution of the OSA is 0.02 nm, the maximum temperature error is ±0.35 ℃ and the maximum strain error is ±4.8 με.

Table 1 presents a comparison of the performance of the proposed sensor with other published sensors of the same class, including the publication year, sensor structure, temperature sensitivity, and strain sensitivity. The proposed in-fiber MZI exhibits the higher sensitivity and better resolution, showcasing promising application prospects in the field of temperature and strain synchronous measurement. Furthermore, the sensor's manufacturing process is much simpler compared to peanut tapers, cascaded structures, and FBGs, which contributes to its cost-effectiveness.

Table 1 Performance comparison with other published sensors.

Publication year	Sensor structure	Temperature sensitivity (pm/℃)	Strain sensitivity (pm/με)
2023	Three cascaded peanut tapers [19]	60.52	−0.911
2023	SMF-TCF-SCPMF-SMF structure [21]	66.7	−1.51
2022	Cascaded SMF and PMF [18]	78.29	−1.441
2020	FBG cascaded TFCF [16]	46.93	1.26
This paper	SMF-FCF-DCF-SMF structure	−94.2	2.68

5. Conclusions

In this paper, an online dual MZI is constructed by cascading two types of optical fibers, FCF, and DCF, for temperature-strain dual-parameter measurement. The maximum temperature sensitivity is −94.2 pm/℃ and the maximum strain sensitivity is 2.68 pm/με. By demodulating the temperature-strain matrix, the simultaneous measurement of two parameters can be realized, and the maximum temperature error of the fabricated sensor is ±0.35 ℃ and the maximum strain error is ±4.8 με. Compared with the similar sensors, this sensor is sensitive, simple, and easy to fabricate, and this sensor will play a great role in future engineering measurement.

Acknowledgment

Partial financial support from Hefei Comprehensive National Science Center is highly appreciated.

This work is supported by the Key Research and Development Plan of Anhui Province (Grant No. 202104a05020059) and Excellent Scientific Research and Innovation Team of Anhui Province (Grant No. 2022AH010003).

Declarations

Conflict of Interest The authors declare that they have no competing interests.

Permissions All the included figures, tables, or text passages that have already been published elsewhere have obtained the permission from the copyright owner(s) for both the print and online format.

References

[1] R. Zhao, G. Shao, Y. Cao, L. An, and C. Xu, "Temperature sensor made of polymer-derived ceramics for high-temperature applications," *Sensors and Actuators: A Physical*, 2014, 219: 58–64.

[2] W. Wildner and D. Drummer, "A fiber optic temperature sensor based on the combination of epoxy and glass particles with different thermo-optic coefficients," *Photonic Sensors*, 2016, 6(4): 295–302.

[3] R. Gao, Y. Jiang, and S. Abdelaziz, "All-fiber magnetic field sensors based on magnetic fluid-filled photonic crystal fibers," *Optics Letters*, 2013, 38(9): 1539–1541.

[4] Q. Bian, A. Podhrazsky, C. Bauer, A. Stadler, F. Buchfellner, R. Kuttler, *et al*., "Temperature and external strain sensing with metal-embedded optical fiber sensors for structural health monitoring," *Optical Express*, 2022, 30(19): 33449–33464.

[5] R. Xu, C. Ke, Y. Xue, Y. Xu, M. Xue, J. Ye, *et al*., "Simultaneous measurement of refractive index and temperature based on SMF-HCF-FCF-HCF-SMF fiber structure," *Sensors*, 2022, 22(22): 8897.

[6] J. Liang, Y. Yu, Q. Bian, W. Xu, Z. Wang, S. Zhang, *et al*., "Metal-coated high-temperature strain optical fiber sensor based on cascaded air-bubble FPI-FBG structure," *Optical Express*, 2023, 31(10): 16795–16811.

[7] H. Xu, F. Li, Y. Gao, and W. Wang, "Simultaneous measurement of tilt and acceleration based on FBG sensor," *IEEE Sensors Journal*, 2020, 20(24): 14857–14864.

[8] J. Liu, Y. Liu, and T. Xu, "Bias error and its thermal drift due to fiber birefringence in interferometric fiber-optic gyroscope," *Optical Fiber Technology*, 2020, 55: 102138.

[9] Q. Bian, C. Bauer, A. Stadler, M. Lindner, M. Jakobi, W. Volk, *et al*., "In-situ high temperature and large strain monitoring during a copper casting process based on regenerated fiber Bragg grating sensors," *Journal of Lightwave Technology*, 2021, 39(20): 6660–6669.

[10] J. Shen, T. Li, H. Zhu, C. Yang, and K. Zhang, "Sensing properties of fused silica single-mode optical fibers based on PPP-BOTDA in high-temperature fields," *Sensors*, 2019, 19(22): 5021.

[11] K. Tian, M. Zhang, Z. Zhao, R. Wang, D. Liu, X. Wang, *et al*., "Ultra-compact in-core-parallel-written FBG and Mach-Zehnder interferometer for simultaneous measurement of strain and temperature," *Optics Letters*, 2021, 46(22): 5595–5598.

[12] Y. Zhao, T. He, M. Chen, Z. B. Zhang, and R. J. Tong, "Ultra-short fiber Bragg grating composed of cascaded microchannels in a microprobe for refractive index measurement," *Journal of Lightwave Technology*, 2023, 41(8): 2555–2561.

[13] H. Gao, H. Hu, Y. Zhao, J. Li, M. Lei, and Y. Zhang,

"Highly-sensitive optical fiber temperature sensors based on PDMS/silica hybrid fiber structures," *Sensors and Actuators A: Physical*, 2018, 284: 22–27.

[14] X. Yang, S. Tang, J. Meng, P. J. Zhang, Y. L. Chen, and Y. F. Xiao, "Phase-transition microcavity laser," *Nano Letters*, 2023, 23(7): 3048–3053.

[15] C. Li, T. Ning, J. Li, L. Pei, C. Zhang, C. Zhang, *et al*., "Simultaneous measurement of refractive index, strain, and temperature based on a four-core fiber combined with a fiber Bragg grating," *Optics & Laser Technology*, 2017, 90: 179–184.

[16] W. Feng, X. Yang, J. Yu, and Z. Yue, "Strain and temperature sensor based on fiber Bragg grating cascaded bi-tapered four-core fiber Mach-Zehnder interferometer," *Journal of Physics D: Applied Physics*, 2020, 53(46): 465104.

[17] J. Tian, Y. Jiao, S. Ji, X. Dong, and Y. Yao, "Cascaded-cavity Fabry-Perot interferometer for simultaneous measurement of temperature and strain with cross-sensitivity compensation," *Optics Communications*, 2018, 412: 121–126.

[18] S. Xiao, B. Wu, Z. Wang, and Y. Jiang, "A peanut taper based Mach-Zehnder interferometric sensor for strain and temperature discrimination," *Optical Fiber Technology*, 2022, 70: 102871.

[19] S. Xiao, B. Wu, C. Sun, Z. Wang, and Y. Jiang. "Strain and temperature discrimination based on a Mach-Zehnder interferometer with cascaded single mode fibers," *Photonic Sensors*, 2023, 13(1): 230122.

[20] J. Ruan, H. Li, and J. Chen, "Strain and temperature discrimination measurement sensor using MMF-PMF-THF fiber structure built in Sagnac loop," *Measurement*, 2023, 207: 112438.

[21] Y. Li, Y. Jiang, N. Tang, G. Wang, J. Tao, and G. Zhang, "Fiber optic temperature and strain sensor using dual Mach-Zehnder interferometers," *Applied Optics*, 2023, 62(8): 1977–1983.

[22] W. Yang, C. Li, M. Wang, X. Yu, J. Fan, Y. Xiong, *et al*., "The polydimethylsiloxane coated fiber optic for all fiber temperature sensing based on the multithin-multifiber structure," *IEEE Sensors Journal*, 2020, 21(1): 51–56.